COMPUTER METHODS IN MATERIALS SCIENCE

2023, vol. 23, no. 4, 31–44
https://doi.org/10.7494/cmms.2023.4.0810

Electrical and thermal analysis for the copper removal process in an electric furnace

Radosław Zybała[1]*, Sławomir Golak[2], Tomasz Sak[1], Piotr Madej[1]

[1] Łukasiewicz Research Network – Institute of Non-Ferrous Metals, ul. Sowińskiego 5, 44-100 Gliwice, Poland.

[2] Department of Industrial Informatics, Faculty of Materials Engineering, Silesian University of Technology, ul. Krasińskiego 8, 40-019 Katowice, Poland.

Abstract

The article presents an electrical model of a resistance furnace with two electrodes encompassing the generation of Joule heat. The characteristic feature of this model was the consideration of contact resistance between the electrodes and the slag. A series of analyses were conducted based on this model.

Firstly, the impact of contact resistance on current flow and Joule heat generation in the furnace was assessed, demonstrating its significant importance. A separate group of analyses focused on the spatial configuration of the furnace and its interaction with the aforementioned phenomena. The impact of symmetric and asymmetric electrodes immersion was analysed. In addition to the impact on current flow, the study also demonstrated the influence on the natural convection mechanism described by the proposed measures of the spatial non-uniformity of heat generation. The research showed that symmetric electrode immersion allows for the generation of more heat in the system at a constant voltage. Asymmetric electrodes immersion causes an increase in the non-uniformity of heat generation, which translates into a higher intensity of natural convection.

Keywords: numerical modelling, copper removal, electric resistance furnace, contact resistance

Introduction

In the process of smelting, a mixture of copper concentrates in single-stage flash smelting technology with the resulting waste slag containing a high concentration of copper (11–15% Cu by weight). The cost-effectiveness of operating single-stage technology is determined by the ability to recover copper from the waste slag. The process is carried out using electric resistance furnaces and is based on the reduction of metal oxides contained in the slag. The product is waste slag depleted to ~0.5% by weight of copper and a metallic alloy containing copper as well as lead and iron.

Decopperisation of slag slurry is a high-temperature process, so thermal phenomena are particularly important. Because the main heat sources present in the process are due to the Joule phenomenon in the flow of electric current through electrodes to the slag, the field of current flow is crucial in analysis. The analyses used an electrical model of a resistance furnace with two electrodes to analyse Joule heat generation, taking into account the contact resistance between the electrode

*Corresponding author: radoslaw.zybala@imn.lukasiewicz.gov.pl
ORCID ID's: 0000-0002-0537-0225 (R. Zybała), 0000-0002-9325-3407 (S. Golak), 0000-0003-0981-1419 (T. Sak), 0000-0002-3019-6572 (P. Madej)

and slag. Figure 1 shows the dimensions of the studied domain, along with an indication of the density of nodes on the given edges of the geometry. The mesh used has 7,582,590 nodes. Table 1 shows the physical parameters used as boundary conditions.

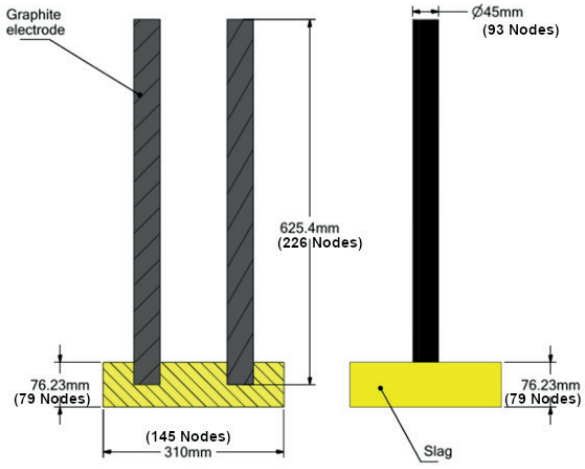

Fig. 1. Main dimensions of the system under study and the used density of mesh nodes

Table 1. Thermophysical properties of the graphite electrodes and slag

Name	Value	Unit
Graphite		
Electric conductivity	125,000	1 / (Ω·m)
Density	1580	kg / m^2
Slag		
Electric conductivity	80	1 / (Ω·m)
Density	3600	kg / m^2

Model of the process

The model was based on Gauss's law of electric current flow. This law describes the electric field generated by the distribution of electric charges. For the analysed electrical furnace system powered by alternating current, the presence of static charges was ignored, defining the field as source-free (Fedosin, 2019; Walker et al., 2014).

$$\nabla \cdot \mathbf{E} = 0 \tag{1}$$

where **E** – electric field intensity; ∇ – Nabla operator.

Due to the modelling of the furnace being powered by alternating current, we use root-mean-square (RMS) values.

$$\mathbf{E} = -\nabla V_E \tag{2}$$

where: V_E – electric potential [V]; ∇ – Nabla operator.

Substituting Equation (2) into the equation describing Gauss's law for electric current flow, it follows that the potential also satisfies Laplace's equation:

$$\nabla \cdot \mathrm{E} = \nabla \cdot (-\nabla V_E) = -\nabla^2 V_E = 0 \tag{3}$$

which, for an inhomogeneous medium inside the furnace, takes the form:

$$\nabla \cdot (\sigma \nabla V_E) = 0 \tag{4}$$

where σ – the electrical conductivity.

The calculated distribution of the root-mean-square values of the electric current allows us to determine the electric field intensity using Equation (2), and then calculate the current density (Tesfahunegn et al., 2018):

$$\mathbf{J} = \sigma \mathbf{E} \tag{5}$$

Joule's law can be expressed as the Ohm's law equation, as all the electric energy in the system is converted into heat. The differential form of the equation for the Joule heating for an infinitely small volume is given by Equation (6) (Amatore et al., 1998).

$$q = \mathbf{J} \cdot \mathbf{E} = \frac{1}{\sigma} \cdot \mathbf{J}^2 \tag{6}$$

The proposed model is a simplified one that describes alternating current using equations for direct current by relying on the RMS values. However, it is representative in terms of the current flow structure and the distribution of Joule heating.

Due to the lack of the direct simulation of current flow in ANSYS Fluent® software, to describe the simplified flow of direct current representing the instantaneous state of the system for alternating current at a given moment in time, it was possible to calculate additional transport equations using user-defined scalars UDS (Ansys, 2022). This mechanism allowed for the solution of the electric potential Equation (4), where V was defined as a user scalar.

Of course, such an approach ignores the presence of the electromagnetic field and the eddy currents generated by it. However, this would require basing the solution used in the modelling of magnetohydrodynamics (MHD) processes (Blacha et al., 2014; Golak & Zagorski, 2013) on the magnetic vector potential, for which the use of additional software dedicated to such tasks is necessary.

However, for the applied frequency of 50 Hz and the size of the analysed laboratory furnace, the electromagnetic field can be neglected without a significant impact on the results (if we are only interested in the structure of the current flow and heat generation).

Effect of the contact layer on heat release

In systems where a fluid comes into contact with a solid body, there is imperfect contact between the two bodies. The resulting layer creates additional resistance called contact resistance, which changes the characteristics of heat or electrical conduction. The phenomenon of contact resistance on the side of the solid body (graphite electrode), in the analysed case, arises due to the rough structure of its surface. On the liquid side, it results from the interaction of the viscosity and surface tension of the liquid, making ideal wetting of the solid body impossible (Thompson & Thompson, 2007; Xia et al., 2022).

To take into account the contact resistance in the graphite electrode – slag system, the modified electrical conductivity of the outer layer of the electrode in contact with the slag is used.

$$\sigma_e = \frac{\sigma_g \cdot l}{l + \sigma_g \cdot R_c} \tag{7}$$

where: σ_g – conductivity of graphite; R_c – conductivity of graphite, l – length of the secant cell in the direction of the current flow (Fig. 2).

This solution allows us to account for the contact resistance in the equation of the electric potential distribution solved using Fluent User Scalars.

The analysed range of contact resistance values was adopted based on data presented in the following publication (Yang et al., 2017). To illustrate the effect of the contact layer on the electric current flow, analyses were conducted for the range of contact resistance R_c from 0 $\Omega \cdot m^2$ to 10^{-5} $\Omega \cdot m^2$ with a constant voltage value of 45 V.

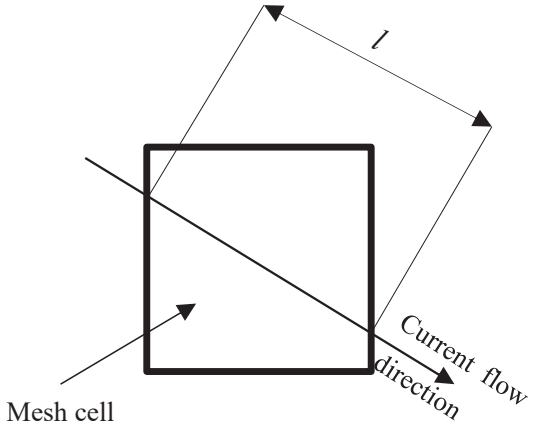

Fig. 2. Diagram describing the dimension l from Equation (7)

Figure 3 shows the change in current flow between the electrodes as a function of the contact layer resistance. From the graph, it can be observed that the amount of current flowing through the slag decreases as the contact resistance value increases. This phenomenon is directly related to Ohm's law describing electrical resistance, where current density decreases as total resistance increases at constant voltage. Some fluctuations in the current density values can be observed in the graph. This increase is caused by numerical artefacts and does not affect the general analysis of the discussed research.

Figure 4 shows a comparison of the current density distribution in the system for the case without taking into account the contact resistance and its maximum value ($R_c = 1 \cdot 10^{-5}$ $\Omega \cdot m^2$). It can be seen that the highest current flow occurs at the entry point of the electrode into the slag. Low current flow occurs at the lower part of the electrode.

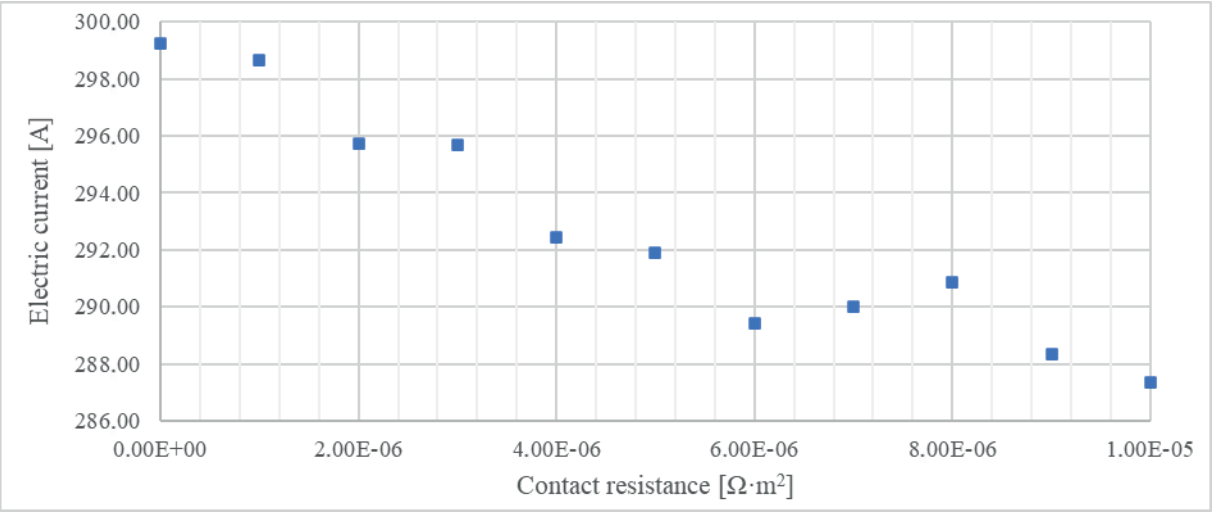

Fig. 3. Graph of the change in the RMS electric current versus contact resistance

Figure 5 show the change in the amount of heat generated as a result of current flow. It can be observed that an increase in the value of the contact resistance causes an increase in the amount of heat generated. The largest amount of heat is generated at the contact layer, where the greatest value in resistances occurs. The average values are presented as numerical values assigned to the measurement points in Figure 5. The Power Density show a rapid increase in the amount of heat released at the already distant lowest contact resistance values.

Figure 6 shows the change in maximum heat generation in the entire volume of the system as a function of the contact resistance value. It can be observed that the highest power density is generated due to the current flow through the slag layer, which is shown by the overlapping of the maximum value curve for the entire volume and for the slag.

The comparison of two extreme cases (Fig. 7) shows a similar overall distribution of heat in the slag, but for the maximum value of contact resistance there is a noticeable increase in the volume in which heat is released, suggesting a significant contribution of the contact layer to heat emission in the slag.

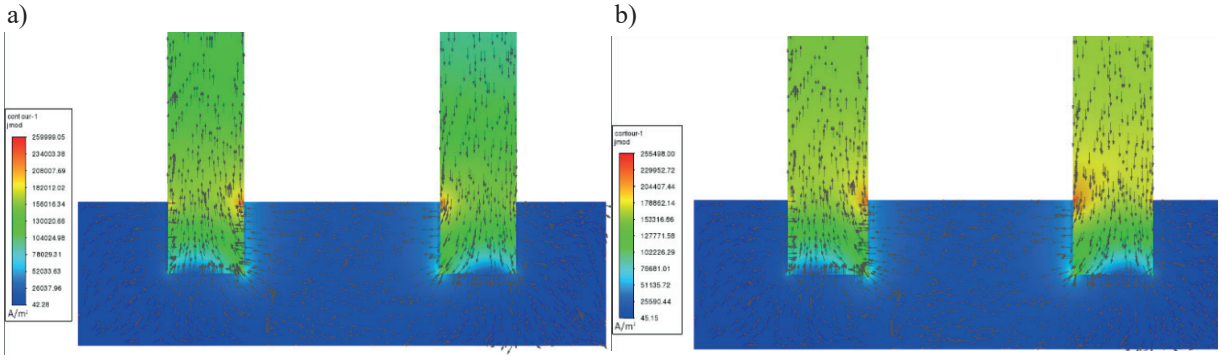

Fig. 4. Distribution of RMS current density in the cross-section together with current flow vectors: a) 0 Ω·m^2 contact resistance, b) $1 \cdot 10^{-5}$ Ω·m^2 contact resistance

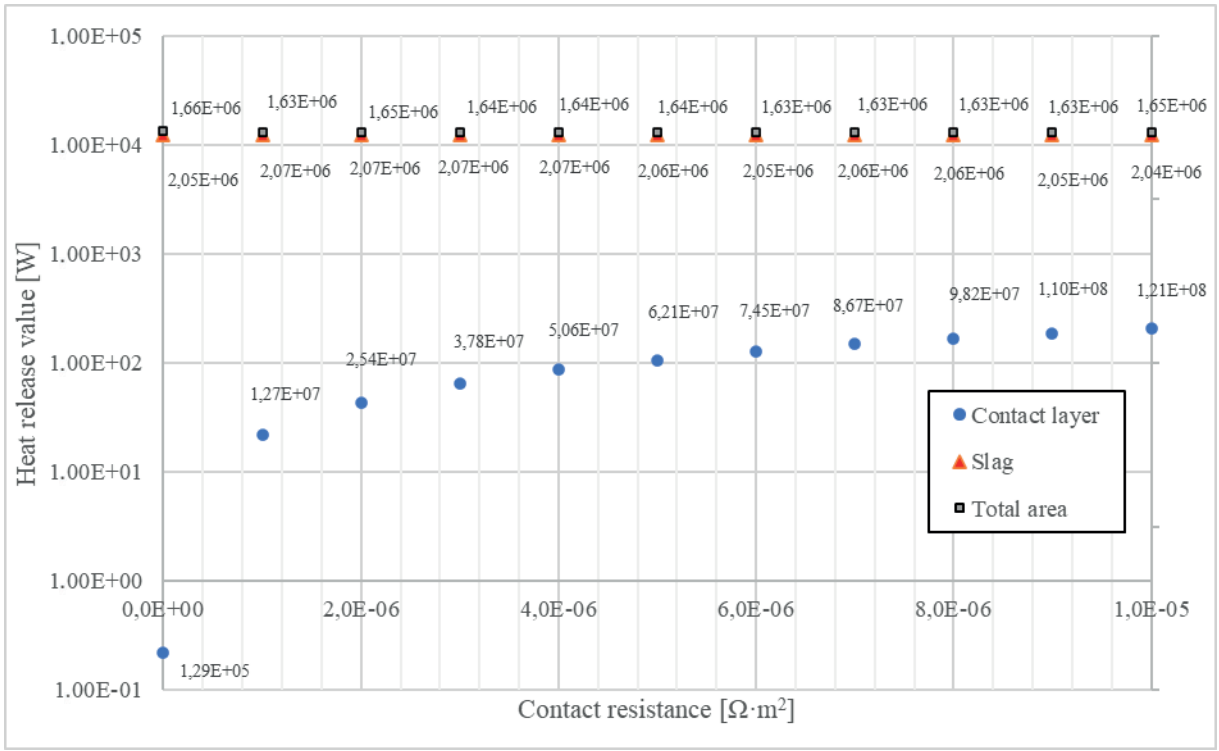

Fig. 5. Dependency of the Joule heat released and its power density (the values at the points [W/m^3])

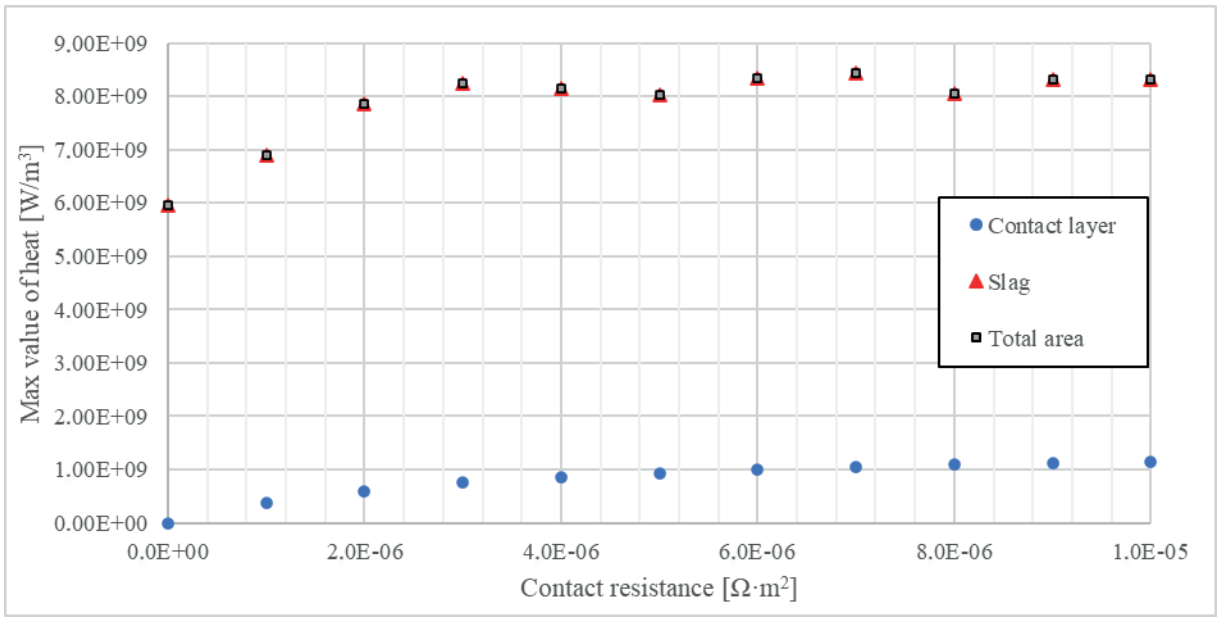

Fig. 6. Dependency of the maximum value of specific power of heat generation on the contact resistance

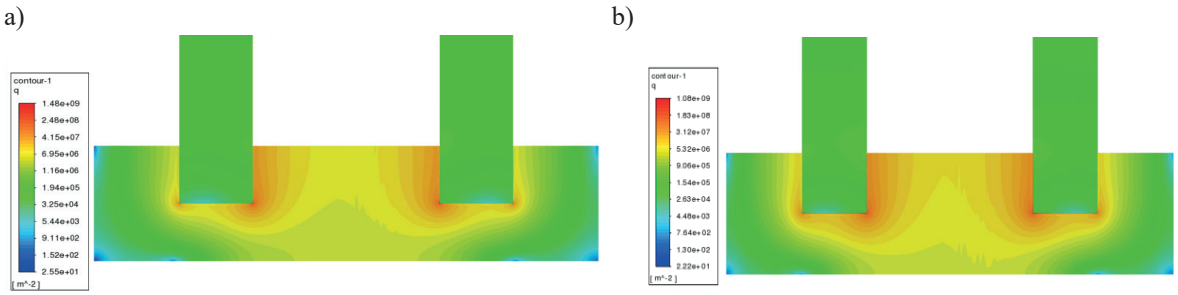

Fig. 7. Heat release intensity distribution in cross-section for 0 Ω·m^2 (a) and $1 \cdot 10^{-5}$ Ω·m^2 (b) contact resistance

The effect of electrode immersion depth on heat release

The second stage of the research aimed to investigate the effect of symmetric immersion of the electrodes on the flow of current and heat generation. The initial state involved electrodes located 0.01 m below the slag level. Then, the electrodes were gradually lowered until they reached a level of 0.07 m below the slag level. In this case, the effect of the contact layer was not taken into account, and the calculations were performed for a constant voltage of 45 V.

Figure 8 shows the change in the value of current flowing as a function of the variable electrode immersion. It can be noticed that with the increase in electrode immersion depth, the current intensity flowing through the slag increases.

Analysing Figure 9, it can be noticed that as the electrodes are submerged more deeply, the flow of electric current stabilizes. There is also an increase in the surface area through which the electric current flows. In order to increase the clarity of the diagram, the colour map range was limited by omitting high current values in the electrode (white area).

As the depth of the electrodes increases, the amount of heat generated inside the slag increases. This is shown in Figures 10 and 11. In Figure 10, a large peak of the released heat value for the entire volume can be observed. However, upon densification of the number of measurement points in this area, it can be noticed that this peak only pertains to a single measurement point which can be disregarded in detailed analyses, as this error arises solely from numerical anomalies. This is related to Joule's law, where the amount of heat generated due to the flow of electric current depends on the square of the current density. This suggests that the immersion of electrodes can be used to control the amount of heat supplied to the system and thus regulate the bath temperature

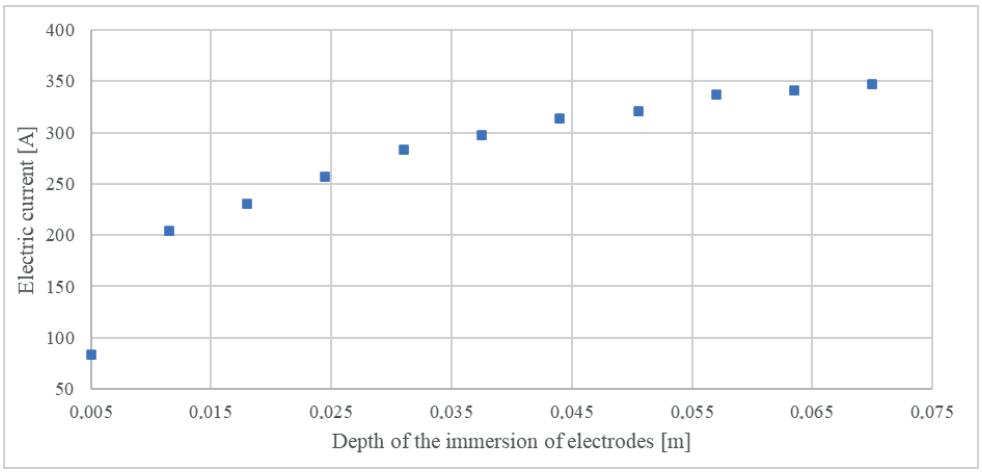

Fig. 8. Graph of the change in the RMS electric current as a function of electrode depth immersion

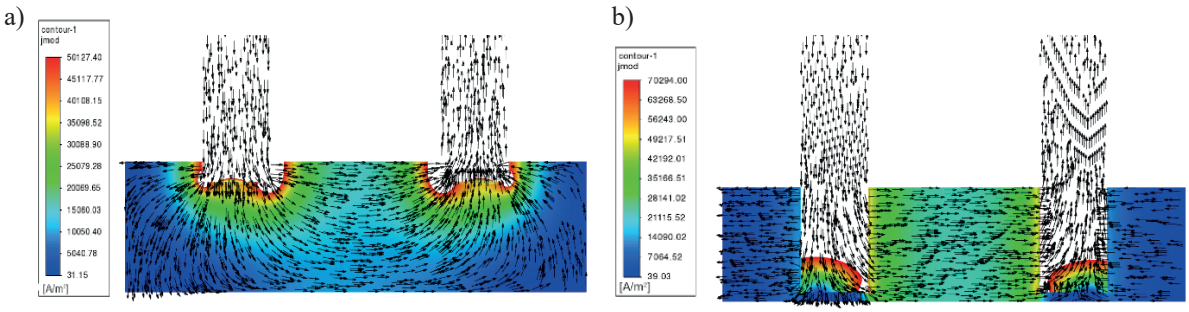

Fig. 9. Distribution of RSM current density in the cross-section together with current flow vectors: a) 0.01 m depth of electrodes immersion; b) 0.07 m depth of electrodes immersion

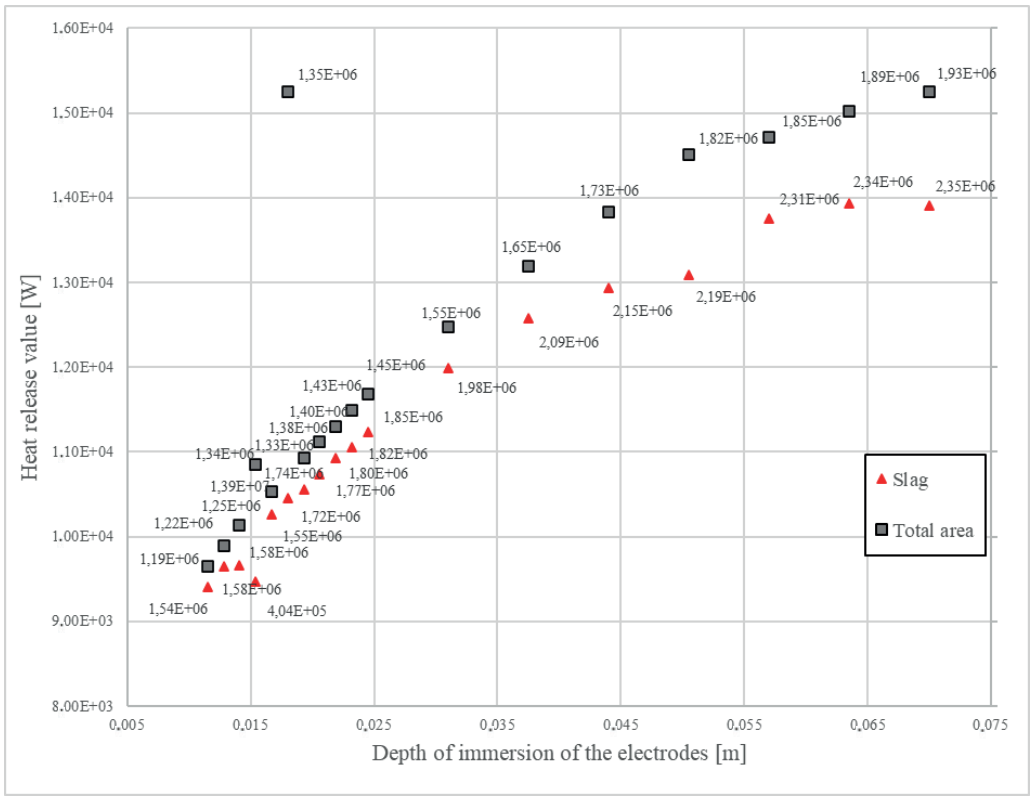

Fig. 10. Dependency of the Joule heat released and its power density (the values at the points [W/m^3]) on the electrodes depth immersion

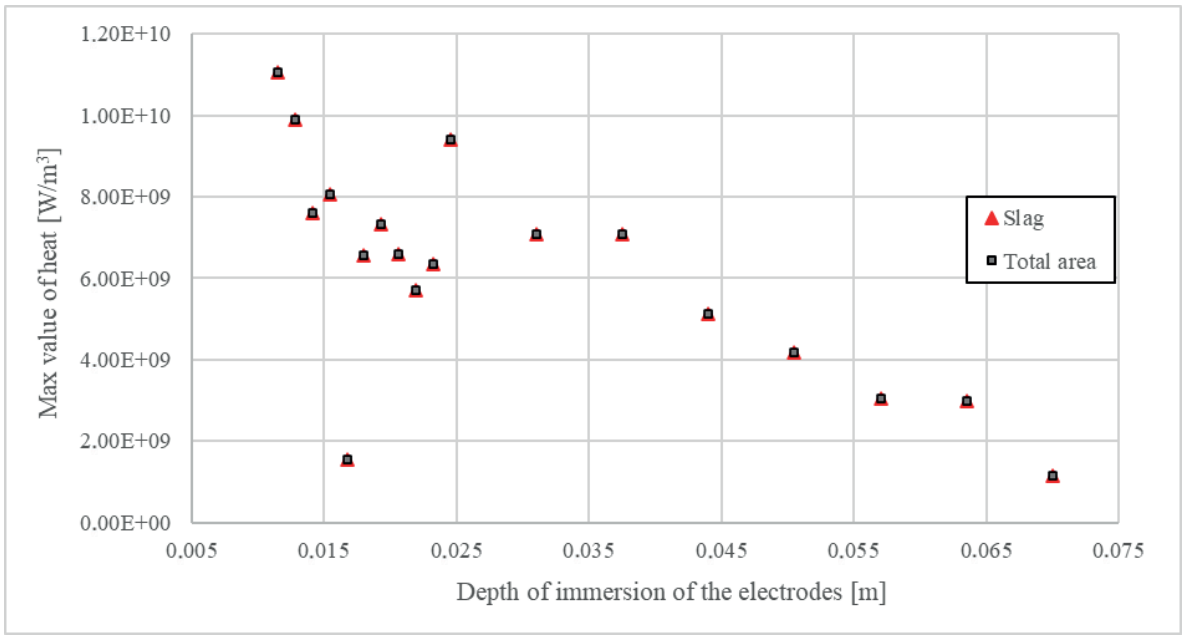

Fig. 11. The maximum value of specific power of heat generation due to the electric current flow on the electrode depth immersion

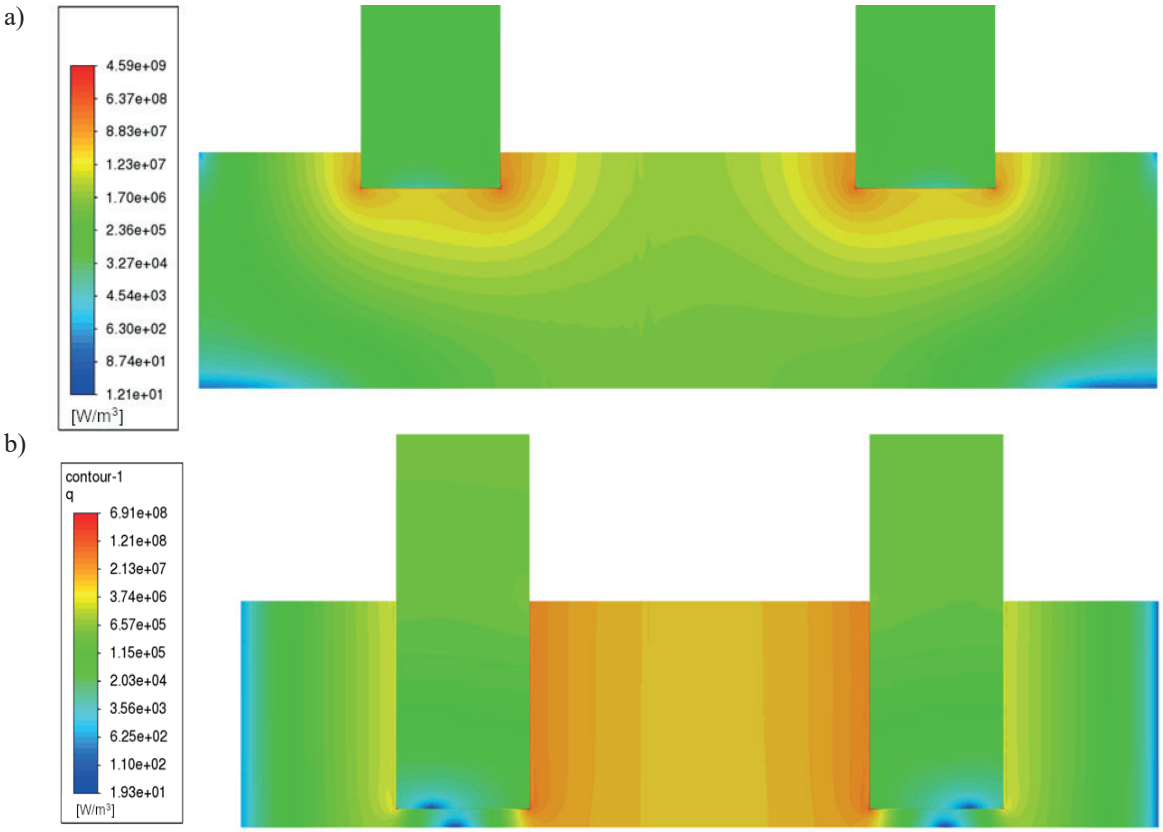

Fig. 12. Heat release intensity distribution in cross-section for:
a) 0.01 m depth of electrode immersion; b) 0.07 m depth of electrode immersion

It can be noticed that maximum immersion results in a significantly higher volume of heat generation in the slag (Fig. 12). However, this may result in the underheating of the bath near the walls, as indicated by the low heat generation marked in blue in Figure 12b.

The next stage of the analysis of this case was to determine the magnitude of the non-uniform distribution of heat in the slag. To this end, analyses were carried out using two methods of determining the non-uniformity of the heat distribution in the slag in accordance with Equations (8) and (9).

Heating of the slag due to the flow of electric current can cause local non-uniformities in the distribution of heat in the slag. Non-uniform heat distribution is the driving force for natural convection. The nature of the heat distribution inside the slag, and hence the temperature distribution, will determine the magnitude of natural convection.

Two methods were used to determine the level of non-uniformity of heat inside the slag:

1. Calculation of the heat gradient integral over the volume of the slag layer.
   The integral of heat gradient represents the overall non-uniformity of the heat distribution inside the slag. It is calculated according to Equation (8).

$$M_1 = \int_V |\nabla q| dV \tag{8}$$

2. Calculation of the standard deviation of heat in the volume of slag.
   Standard deviation of the heat distribution in the slag represents local non-uniformities of heat in this material.

$$M_2 = \sqrt{\frac{1}{V}\int_V (q-\bar{q})^2 dV} \tag{9}$$

The results obtained using Equation (8) are presented in Figures 13 and 14. Figure 15 shows the second method of determining the non-uniformity of heat in slag according to Equation (9).

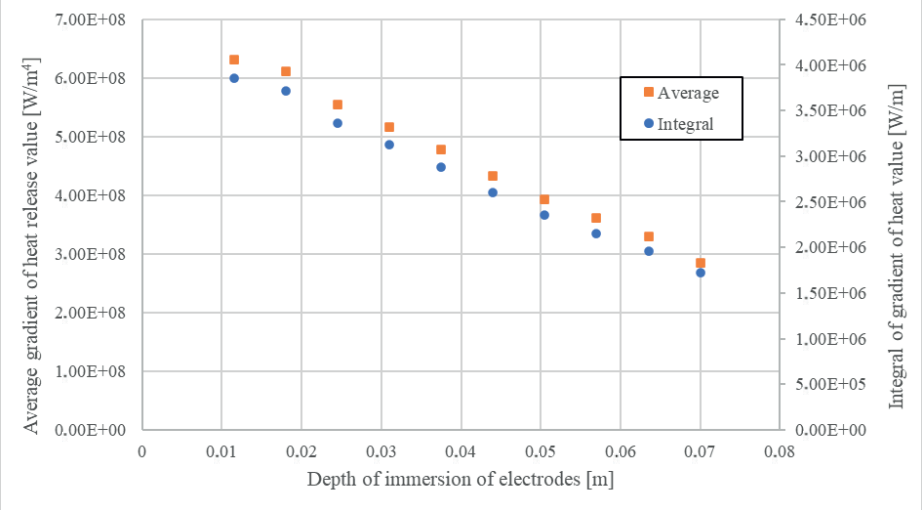

Fig. 13. Plot of the integral and average of the heat gradient as a function of electrode depth immersion

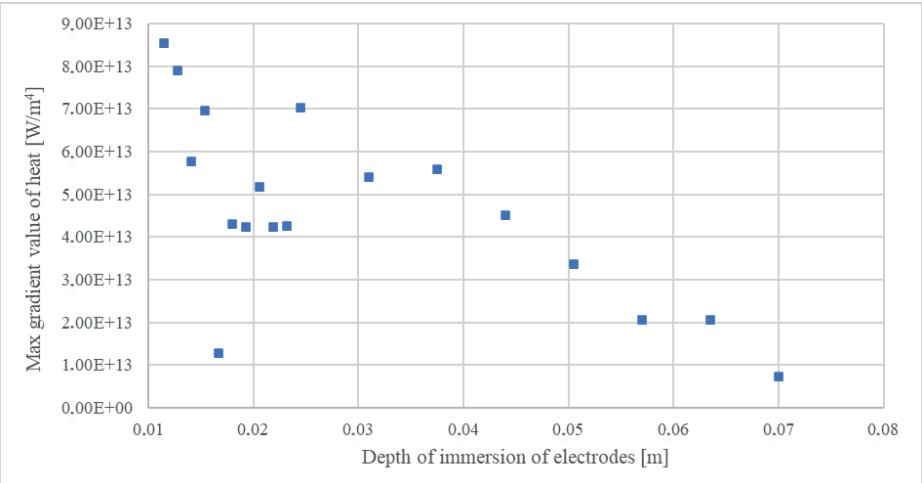

Fig. 14. Plot of the maximum value of heat gradient as a function of electrode depth immersion

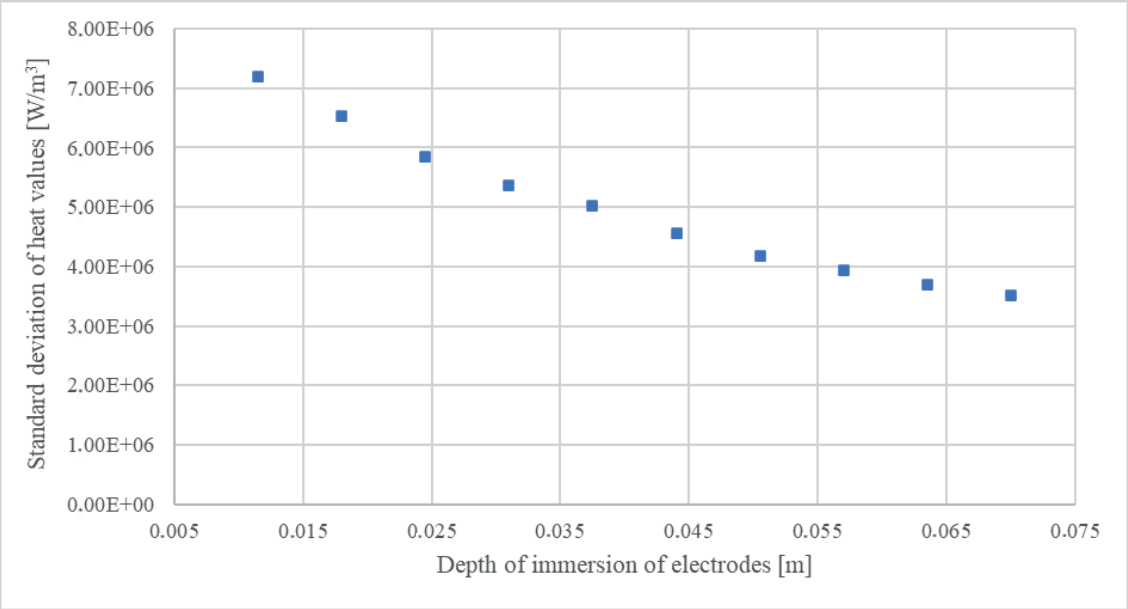

Fig. 15. Plot of the standard deviation of heat gradient as a function of electrode depth immersion

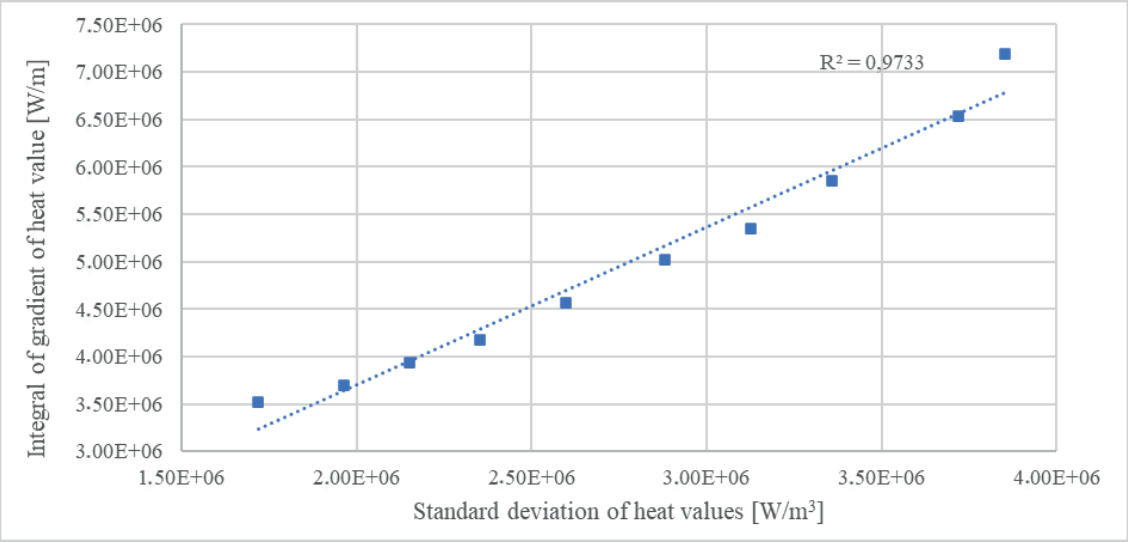

Fig. 16. Plot of correlation between the integral of gradient of heat and the standard deviation of heat

As immersion depth increases, the non-uniformity of the generated heat decreases. This will cause a reduction in the driving force of natural convection. With the increase in electrode immersion, the natural mixing of the slag will be reduced. The non-uniform change in the maximum electric current value is caused by numerical artefacts and does not affect the entire analysis.

Figure 16 presents a correlation plot of the heat gradient integral and standard deviation. As a result of the calculations, a correlation coefficient of 0.97 was obtained, indicating that both methods for determining heat non-uniformity can be used interchangeably.

The effect of asymmetrical immersion of electrodes on heat release

The last stage of the study was to investigate the effect of asymmetric electrode displacement on current flow and heat generation in the slag. The starting point was the arrangement of electrodes submerged halfway into the bath, and the end point was the placement of one electrode 0.005 m below the surface of the melt and the other 0.005 m above the bottom of the crucible.

Stretching the electrodes causes a decrease in the current flowing through, as illustrated in Figure 17. This is caused by the elongation of the path that the electron must travel from one electrode to the other.

This is well shown in Figure 18, where a change in the path of current vectors inside the slag can be observed. This illustration also clearly shows the change in the electrode surface area through which the charge enters the bath.

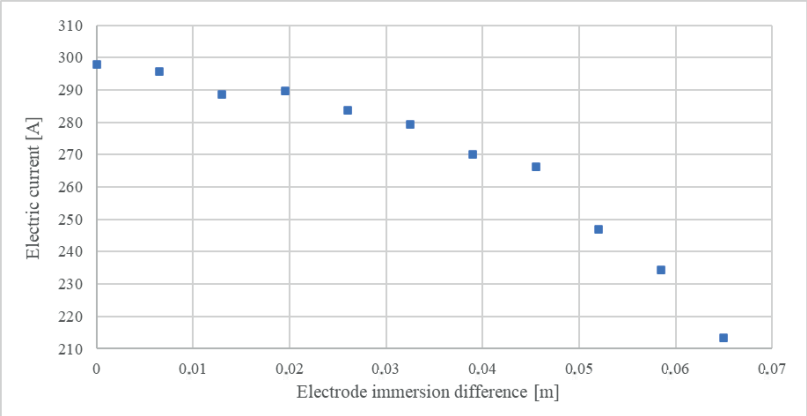

Fig. 17. Graph of the change in the RMS electric current as a function of electrode immersion difference

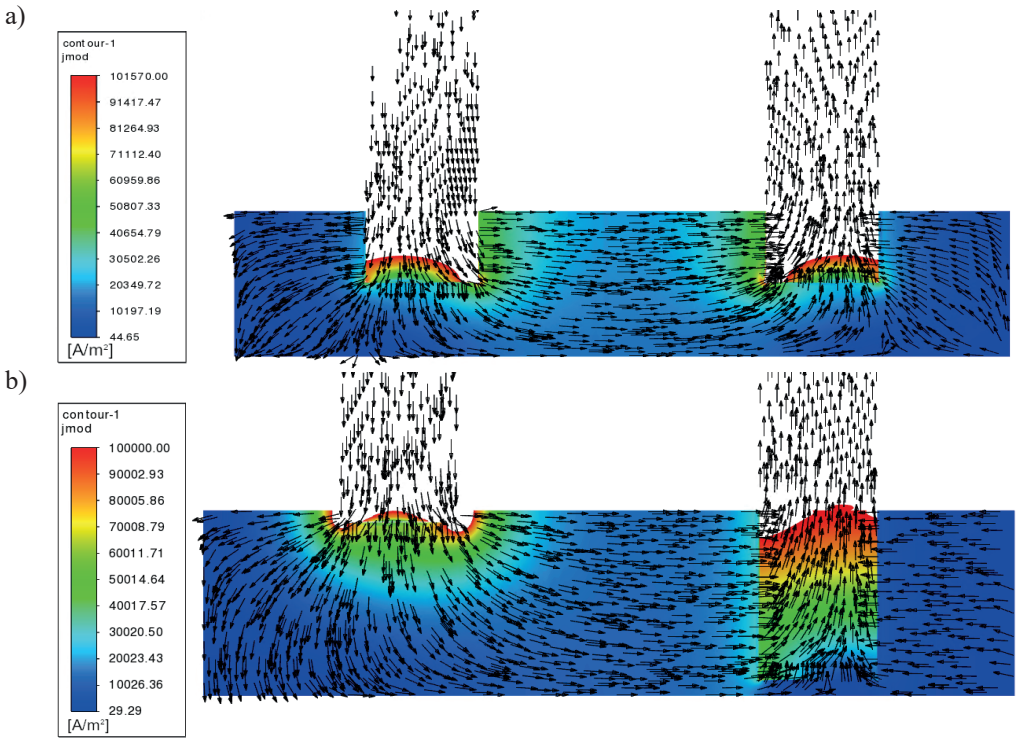

Fig. 18. Distribution of current density in the cross-section together with current flow vectors: a) 0 m electrode immersion difference; b) 0.065 m electrode immersion difference

The analysis of the amount of heat generated due to the flow of electric current indicates a decrease in its quantity with the spreading apart of the electrodes, as shown in Figures 19 and 20. Figure 19 shows the changes in heat emission values and, in the form of numerical values assigned to points, the average values. The reduced amount of heat is due to a lower value of current density inside the slag. An interesting observation is the increase in the maximum value of generated heat shown in Figure 20, despite the overall decrease in the amount of heat in the system.

This is most likely the effect of the shallow immersion of one of the electrodes, which, in conjunction with the previously indicated phenomenon of the greatest heat generation at the entry point of the electrode into the slag, produces such an effect.

The decrease in the amount of generated heat is well shown in Figure 21. It can be observed that in Figure 21b, there is a small amount of heat generated on the wall of the bath near the submerged electrode, indicating a low current flow in that part of the bath. Shallow submerging of the electrode causes the current to flow through the entire contact volume with the slag, improving the heat transport in the upper corner of the bath.

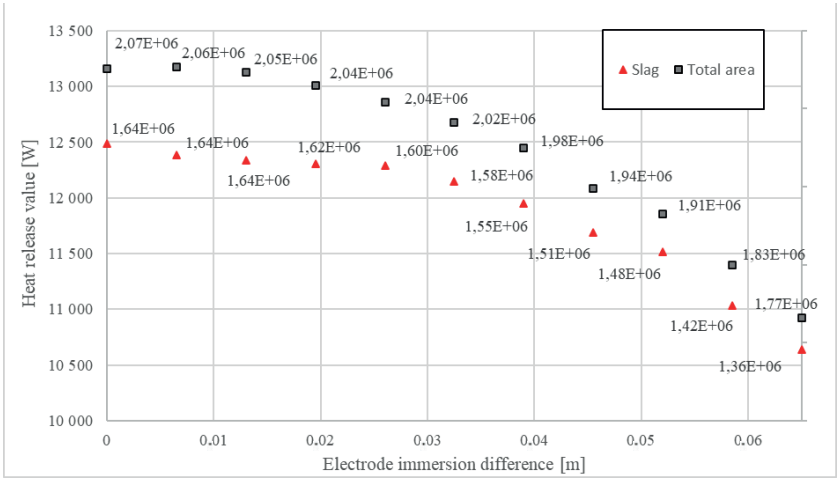

Fig. 19. Dependency of the Joule heat released and its power density (the values at the points [W/m^3]) on the electrode immersion difference

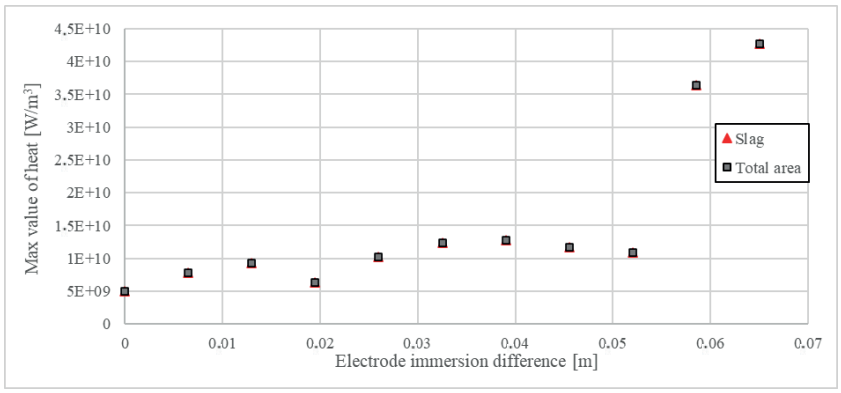

Fig. 20. The maximum value of specific power of heat generation due to the electric current flow as a function of the electrode immersion difference

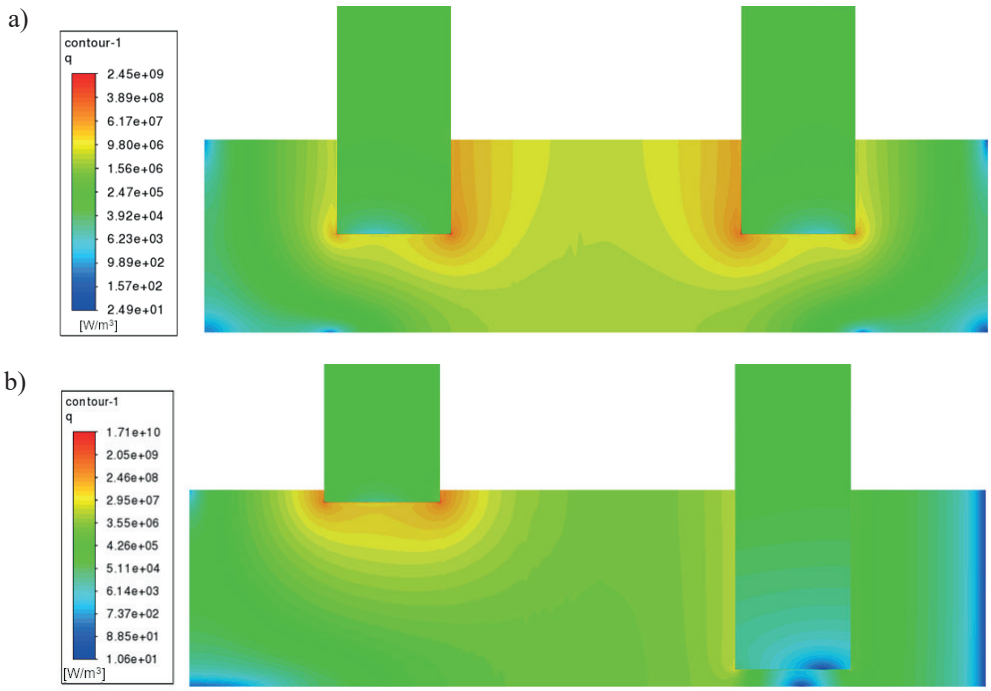

Fig. 21. Heat release intensity distribution in the cross-section for:
a) 0 m electrode immersion difference; b) 0.065 m electrodes immersion difference

Similarly to the previous case, analyses of the non-uniformity of heat distribution in the slag were also carried out, which are presented in Figures 22–24. In the analysed case, an increase in the non-uniformity of heat distribution is noticeable, which will result in intensified natural convection in the system.

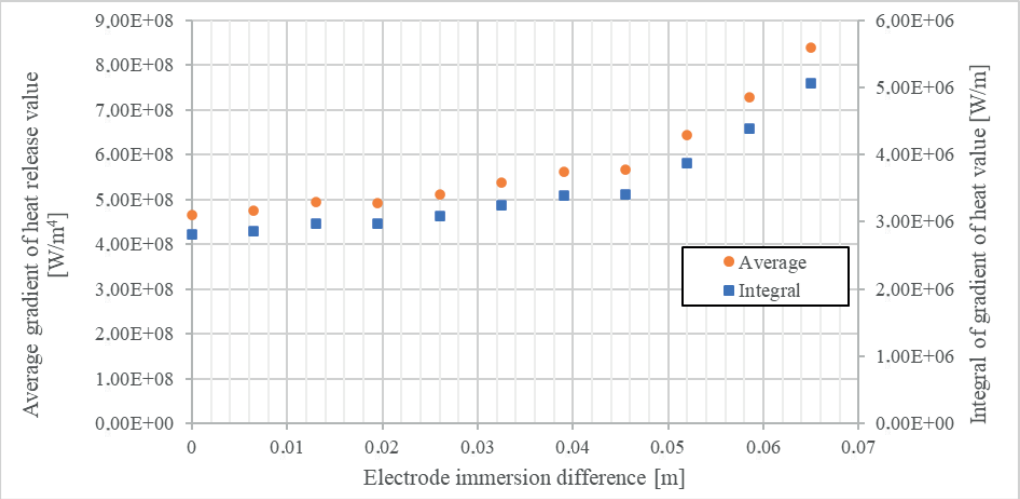

Fig. 22. Plot of the integral and average of the heat gradient as a function of the electrodes immersion difference

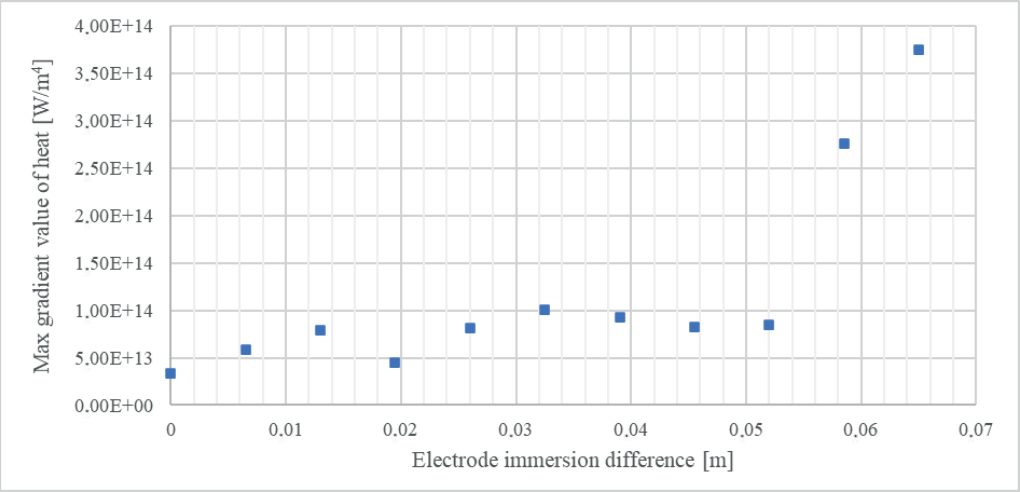

Fig. 23. Plot of the maximum value of heat gradient as a function of the electrode immersion difference

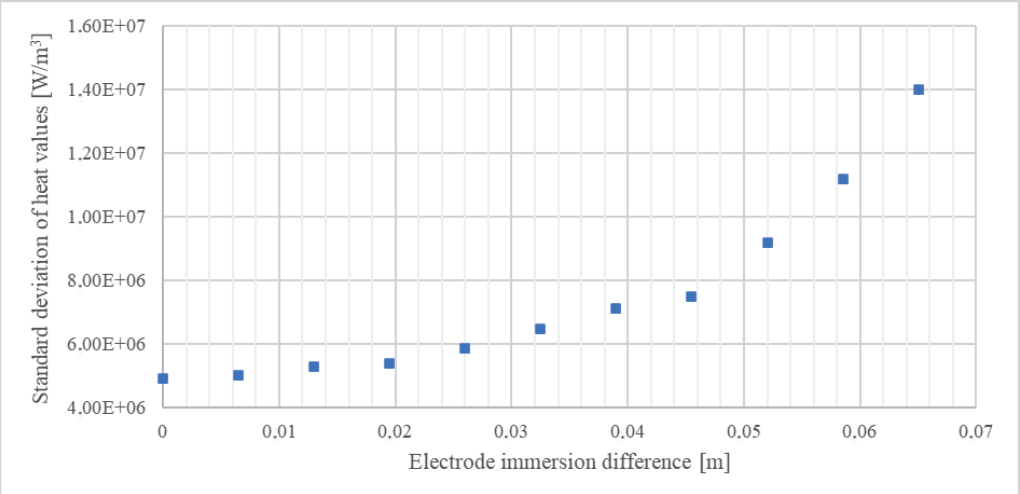

Fig. 24. Plot of the standard deviation of heat gradient as a function of the electrode immersion difference

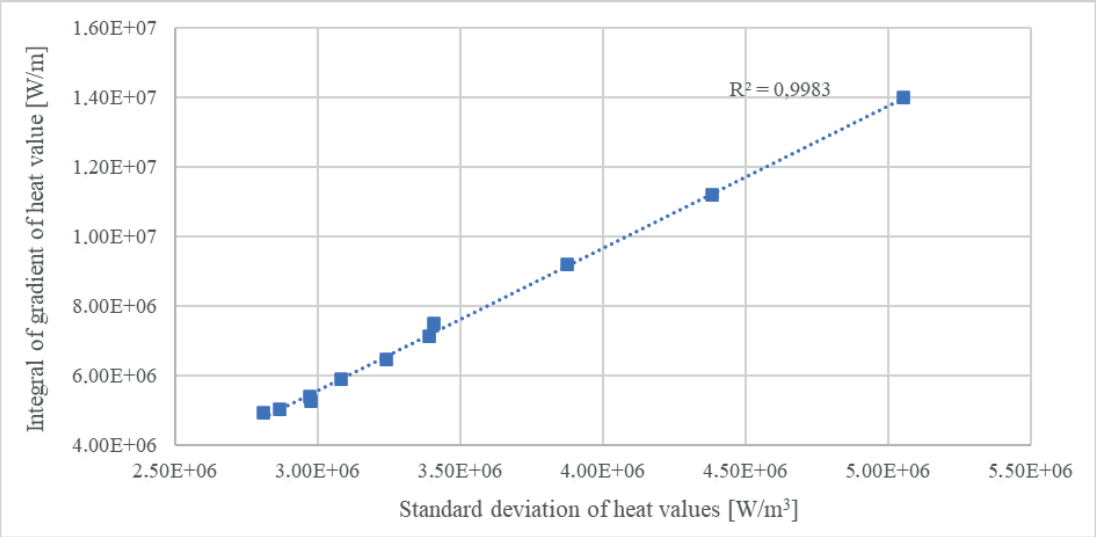

Fig. 25. Plot of correlation between the integral of gradient of heat and the standard deviation of heat

Figure 25 presents a correlation plot between the integral of heat gradient and standard deviation. The obtained correlation is at the level of 0.998, indicating that both methods of determining heat non-uniformity can be used interchangeably.

Conclusions

The article presents a simplified electrical model of an electric furnace, which, despite omitting some phenomena, such as the electromagnetic field and hydrodynamics of liquid slag, allowed for conducting analyses that provided interesting results concerning both the modelling procedure and furnace configuration of the furnace by manipulating the immersion of electrodes.

The presented analyses indicate the justification of considering the properties of the contact layer between the electrode and slag. This is indicated by the decrease in the value of electric current through the slag at constant voltage.

The analysis of the symmetric electrode immersion case showed an increase in the current flow through the slag and thus an increase in the amount of heat generated. Such a displacement of the electrodes will worsen the mixing conditions of the bath by natural convection forces.

Asymmetric immersion of electrodes results in a decrease in electric current flow, which leads to a lower amount of heat generated in the slag. However, such an electrode configuration increases the non-uniformity of heat distribution, which positively affects slag mixing due to natural convection.

The presented analyses will in the future require comparison with results provided by models that take into account the hydrodynamics of the slag and electromagnetic field.

References

Amatore, C., Berthou, M., & Hébert, S. (1998). Fundamental principles of electrochemical ohmic heating of solutions. *Journal of Electroanalytical Chemistry*, *457*(1–2), 191–203. https://doi.org/10.1016/S0022-0728(98)00306-4.

Ansys (2022). *Ansys Fluent Theory Guide R2*. https://download.ansys.com/Product%20Documentation.

Blacha, L., Golak, S., Jakovics, A., & Tucs, A. (2014). Kinetic analysis of aluminium evaporation from the Ti-6Al-7Nb alloy. *Archives of Metallurgy and Materials*, *59*(1), 275–279. https://doi.org/10.2478/amm-2014-0045.

Fedosin, S.G. (2019). On the covariant representation of integral equations of the electromagnetic field. *Progress in Electromagnetics Research C*, *96*, 109–122. https://doi.org/10.2528/PIERC19062902.

Golak, S., & Zagorski, R. (2013). Model and optimization of electromagnetic filtration of metals. *Metalurgija*, *52*(2), 215–218.

Tesfahunegn, Y.A., Saevarsdottir, G., Magnusson, T., & Tangstad, M. (2018). The effect of frequency on current distributions inside submerged arc furnace. In *2018 IEEE MTT-S International Conference on Numerical Electromagnetic and Multiphysics Modeling and Optimization (NEMO)* (pp. 1–4). IEEE. https://doi.org/10.1109/NEMO.2018.8503083.

Thompson, M.K., & Thompson, J.M. (2007). Considerations for predicting thermal contact resistance in ANSYS. In *17th KOREA ANSYS User's Conference*. https://www.researchgate.net/publication/280626733_Considerations_for_Predicting_Thermal_Contact_Resistance_in_ANSYS.

Walker, J., Halliday, D., & Resnick, R. (2014). *Fundamentals of Physics* (10th ed.). John Wiley & Sons.

Xia, G., Tuo, W., Li, X., & Liu, X. (2022). Study on the performance of liquid-solid contact resistance based on magnetohydrodynamic micro-angular vibration sensor. *Sensors*, *22*(23), 9204. https://doi.org/10.3390/s22239204.

Yang, H., Wolters, J., Pischke, P., Soltner, H., Eckert, S., Natour, G., & Fröhlich, J. (2017). Modelling and simulation of a copper slag cleaning process improved by electromagnetic stirring. In *IOP Conference Series: Materials Science and Engineering* (vol. 228). https://doi.org/10.1088/1757-899X/228/1/012007.